


RESEARCH ARTICLE

Sulfatase 2 promotes generation of a spinal cord astrocyte subtype that stands out through the expression of Olig2

David Ohayon | Nathalie Escalas | Philippe Cochard | Bruno Glise |
Cathy Danesin | Cathy Soula 

Centre de Biologie du Développement (CBD)
CNRS/UPS, Centre de Biologie Intégrative
(CBI), Université de Toulouse, Toulouse,
France

Correspondence

Cathy Soula, Centre de Biologie du
Développement (CBD) CNRS/UPS, Centre de
Biologie Intégrative (CBI), Université de
Toulouse, Toulouse, France.
Email: catherine.soula@univ-tlse3.fr

Funding information

Agence Nationale de la Recherche, Grant/
Award Number: ANR-15-CE16-0014-02;
Centre National de la Recherche Scientifique;
Fondation ARC pour la Recherche sur le
Cancer; Fondation pour l'Aide à la Recherche
sur la Sclérose en Plaques; Université de
Toulouse

Abstract

Generation of glial cell diversity in the developing spinal cord is known to depend on spatio-temporal patterning programs. In particular, expression of the transcription factor Olig2 in neural progenitors of the pMN domain is recognized as critical to their fate choice decision to form oligodendrocyte precursor cells (OPCs) instead of astrocyte precursors (APs). However, generating some confusion, lineage-tracing studies of Olig2 progenitors in the spinal cord provided evidence that these progenitors also generate some astrocytes. Here, we addressed the role of the heparan sulfate-editing enzyme Sulf2 in the control of gliogenesis and found an unanticipated function for this enzyme. At initiation of gliogenesis in mouse, Sulf2 is expressed in ventral neural progenitors of the embryonic spinal cord, including in Olig2-expressing cells of the pMN domain. We found that *sulf2* deletion, while not affecting OPC production, impairs generation of a previously unknown Olig2-expressing pMN-derived cell subtype that, in contrast to OPCs, does not upregulate Sox10, PDGFR α or Olig1. Instead, these cells activate expression of AP identity genes, including *aldh1L1* and *fgfr3* and, of note, retain Olig2 expression as they populate the spinal parenchyma at embryonic stages but also as they differentiate into mature astrocytes at postnatal stages. Thus, our study, by revealing the existence of Olig2-expressing APs that segregate early from pMN cells under the influence of Sulf2, supports the existence of a common source of APs and OPCs in the ventral spinal cord and highlights divergent regulatory mechanism for the development of pMN-derived OPCs and APs.

KEYWORDS

astrocyte, gliogenesis, olig2, oligodendrocyte, spinal cord, sulfatase 2

1 | INTRODUCTION

Glial cells are recognized for serving critical functions in the central nervous system (CNS). Among them, astrocytes and oligodendrocytes, namely glial cells of neural origin, populate all regions of the mature CNS. Astrocytes are active regulators of synaptogenesis and neurotransmission and are also critical for formation of the blood–brain

barrier. The mostly known feature of oligodendrocytes is formation of myelin sheaths that provides insulation of neuronal axons.

Acquisition of these two distinct glial cell fates is acknowledged to result from spatial segregation of neural progenitors that is established early, during patterning of the neural tube. A good understanding of organizing signals and target genes involved in this process was acquired studying the development of the embryonic spinal cord

This is an open access article under the terms of the Creative Commons Attribution-NonCommercial-NoDerivs License, which permits use and distribution in any medium, provided the original work is properly cited, the use is non-commercial and no modifications or adaptations are made.

© 2019 The Authors. *Glia* published by Wiley Periodicals, Inc.

(Dessaud, McMahon, & Briscoe, 2008). Under the influence of patterning signals, progenitor cells of the ventral neural tube activate or repress sets of transcription factors that subsequently subdivide this structure into distinct progenitor domains, each dedicated to first generate specific neuronal subtypes, followed by glial cells (Ben Haim & Rowitch, 2017). Among them, the pMN domain, populated by progenitor cells expressing the transcription factor Olig2, first generates all motor neurons (MNs) and change with time to produce most oligodendrocyte precursor cells (OPCs) of the spinal cord. Meanwhile, the ventrally and dorsally located p1 to p3 domains initially produce V1 to V3 interneurons and then change their fate to generate three distinct ventral astrocyte precursor cell (AP) subtypes (VA1-3). Thus, the origins of OPCs and APs are considered to be more closely connected to neuron subtype progenitor cells than with each other. The mechanistic parallel between neuron and glial cell development is well exemplified by functional analysis of the transcription factor Olig2, expressed in pMN cells. In Olig2 null spinal cords, pMN cells fail to generate both MNs and OPCs (Lu et al., 2002; Takebayashi, Nabeshima, Yoshida, Chisaka, & Ikenaka, 2002; Zhou & Anderson, 2002). Instead, in these mutants, supernumerary V2 interneurons and APs are produced as a consequence of transformation of the presumptive pMN domain into a p2 domain. Therefore, spinal OPCs and APs have been proposed to develop along mutually exclusive paths, Olig2 being viewed as a repressor of a “pro-astrocytic” program (Rowitch & Kriegstein, 2010). Olig2 is also considered as a key determinant of OPC specification, maturation, and differentiation and it continues to be present in differentiated oligodendrocytes of the adult spinal cord (Meijer et al., 2012). However, contrasting with the notion that Olig2 represses the astrocytic fate, lineage-tracing studies brought evidence that Olig2-expressing progenitors of the pMN domain generate some astrocytes (Masahira et al., 2006; Tsai et al., 2012).

Beyond spatial control, a temporal component is important to initiate gliogenesis. Although timing mechanism regulating AP commitment remains elusive, OPC commitment from pMN cells is known to rely on a temporal rise of sonic hedgehog (Shh) signaling activity (Danesin & Soula, 2017). The heparan sulfate-editing enzyme Sulf1, known to modulate the sulfation state of heparan sulfate proteoglycans (HSPGs) at the cell surface (Lamanna et al., 2007), is a key player in this process. This enzyme is expressed specifically by Shh-secreting cells of the floor plate immediately prior to OPC specification. Sulf1, by eliminating 6O sulfate groups on HS chains, locally lowers Shh/HSPG interaction and thereby promotes Shh release at the right time to trigger OPC specification from Olig2-expressing pMN cells (Al Oustah et al., 2014; Touahri et al., 2012). Jiang et al. (2017) more recently reported that Sulf2, the second member of the Sulf protein family (El Masri, Seffouh, Lortat-Jacob, & Vivès, 2017), plays a similar role as Sulf1 in triggering the MN to OPC fate change. In the present work, we also investigated the function of Sulf2 in the control of gliogenesis during spinal cord development and came to the different conclusion that Sulf2 is dispensable for OPC production. Instead, we found that Sulf2, which in contrast to Sulf1 is expressed in pMN cells, promotes generation of APs. Furthermore, we showed that APs generated under the influence of Sulf2 are distinguishable from other APs by the expression of Olig2 from

initial stages of their generation in the ventral spinal cord to their final maturation at postnatal stages. These results therefore reveal a previously uncharacterized spinal cord AP subtype characterized by expression of Olig2. By highlighting the role of Sulf2 in this glial subtype development, our data also reveal distinct developmental mechanisms for generation of OPC and AP from progenitor cells of the pMN domain.

2 | MATERIALS AND METHODS

2.1 | Mouse strains

All procedures were performed in agreement with the European Community guiding principles on the care and use of animals (Scientific Procedures) Act, 1987 and approved by the national Animal Care and Ethics Committee (APAFIS#01331.02) following Directive 2010/63/EU. Sulf2 mutant and floxed mice have been generated by Ai et al. (2007). Sulf2 mutant carry deletion of the second coding exon (exon 2) of *sulf2*, which encodes essential amino acids in the enzymatic domain of the protein (Dhoot et al., 2001). Sulf2 floxed mice carry LoxP sites flanking the exon2 of *sulf2*. Sulf2 mutant and floxed mice were genotyped as previously reported (Ai et al., 2007; Tran, Shi, Zaia, & Ai, 2012). Parental *olig2-cre^{+/-};sulf2^{fl/+};R26R-tomato* mice were generated by crossing heterozygous knock-in *olig2-cre* line (Dessaud et al., 2007) with mice carrying one floxed *sulf2* allele and the R26R-tomato reporter (*sulf2^{fl/+}; R26R-tomato*). *Olig2-cre^{+/-}; sulf2^{fl/+}; R26R-tomato* mice were crossed and *olig2-cre^{+/-}; sulf2^{fl/+}; R26R-tomato* and *olig2-cre^{+/-}; sulf2^{fl/+}; R26R-tomato* littermate embryos were selected by genotyping. GFAP-GFP and Aldh1L1-GFP transgenic mice were genotyped as previously reported (Gong et al., 2003; Heintz, 2004; Nolte et al., 2001). Parental *sulf2^{+/-}; Aldh1L1-GFP* mice were generated by crossing heterozygous *sulf2* mutant mouse to an *Aldh1L1-GFP* transgenic mouse. Then, *sulf2^{+/-}; Aldh1L1-GFP* mice were crossed and *sulf2^{+/+}; Aldh1L1-GFP* and *sulf2^{-/-}; Aldh1L1-GFP* littermate embryos were selected by genotyping. All mice were maintained on a C57BL/6 background.

2.2 | Thymidine analogue labeling

For proliferation assays, the timed pups (P0) were injected intraperitoneally with 5-ethyl-2-deoxyuridine (EdU, Invitrogen) at 50 µg/g body weight once a day from postnatal Day 0 to postnatal Day 2. The animals were then sacrificed 2 hr after the last injection. EdU incorporation was detected using the AlexaFluor-647 Click-iT Imaging Kit (Invitrogen).

2.3 | Tissue processing

Spinal cords at the brachial level were isolated from E12.5 to E18.5 mouse embryos and fixed in 4% paraformaldehyde (PFA, Sigma) in phosphate-buffered saline (PBS) overnight at 4 °C. Adult mice were perfused intracardially with 4% PFA (Sigma) in PBS. Adult spinal cords were dissected and postfixed in 4% PFA in PBS overnight at 4 °C. Tissues were then sectioned either at 60–80 µm using a vibratome

(Microm) or at 15 to 25 μm using a cryostat (Leica CM1950) after cryoprotection in 20% sucrose (Sigma) in PBS and freezing in OCT media on the surface of dry ice.

2.4 | In situ RNA hybridization and immunofluorescent staining

Simple or double in situ hybridization and immunofluorescent staining were performed on transverse sections as previously reported (Touahri et al., 2012; Ventéo et al., 2012). Digoxigenin- or Fluorescein-labeled antisens RNA probes for *sulf2*, *aldh1L1*, *fgfr3*, *sox10*, and *tenascin-C* were synthesized using DIG- or Fluorescein-labelling kit (Roche) according to the manufacturer's instructions and revealed using either NBT/BCIP (Roche), INT/BCIP (Roche) or Alexa-fluor 488 Tyramide (Molecular Probes). Antibodies used in this study were as follows: goat anti-AldoC (Santa Cruz Biotechnology), rabbit and mouse anti-GFAP (DAKO), rabbit anti-NFIA (Active Motif), rabbit and goat anti-Olig2 (Millipore and R&D Systems), goat anti-Olig1 (R&D Systems), goat anti-Sox10 (Santa Cruz Biotechnology), rat anti-PDGFR α (BD Pharmingen), rabbit anti-Zeb1 (Novus), mouse anti-Nkx6.1 (Hybridoma Bank), mouse anti-Cx43 (BD Biosciences) and rabbit anti-Cx30 (Thermo Fisher Scientific). Alexa Fluor-594- or Alexa Fluor-488 or Alexa Fluor-647-conjugated secondary antibodies (Thermo Fisher Scientific) were used.

2.5 | Imaging, cell counting, and statistical analysis

Confocal images were acquired from tissue sections using Leica SP5 or SP8 confocal microscopes and were always represented as single optical plane sections. In some instances, Z-stacks were acquired at high magnification ($\times 63$ objective) and images along the Z-axis were obtained using the Reslice feature of ImageJ software along a straight or broken line drawn in the X/Y plane. Images of simple or double bright-field ISHs were collected with Nikon digital camera DXM1200C on a Nikon Eclipse 80i microscope. Double ISH stainings and double ISH-immunofluorescence staining were imaged on Leica SP5 confocal microscope according to the method of Trinh et al. (2007) which allows acquiring in the same optical plane a high resolution confocal image of NBT/BCIP stain in the near infrared range together with the immunofluorescence or TSA signals. Images were processed (size adjustment, luminosity and contrast, and merging or separating layers) using Adobe Photoshop CS6 software (Adobe). Provided data are the average of four to eight individuals per condition. Numbers of individuals (n) are indicated in figure legends. Cell counts were performed using ImageJ software and obtained from at least five tissue sections of brachial spinal cord (anterior limb level). For each 60–80 μm tissue slice, at least four optical sections were acquired at 6 μm intervals and cells were counted in each optical section. The same approach was applied for each 15–25 μm tissue slices except that only two optical sections were used. For regional cell number quantification at embryonic and postnatal stages, distribution of cells in the ventral spinal cord was obtained by drawing a straight line through the midline dividing the spinal cord into two equal regions. Cell counts on adult spinal cord sections were limited to the ventral horns. Quantifications are expressed as the mean

number of cells (mean \pm SEM) in an optical section of hemi-ventral spinal cord sections. Statistical analyses were performed using the Mann-Whitney *U* test on Prism software (GraphPad). Significance was determined at $p < .05$. *p* values are indicated in figure legends.

3 | RESULTS

3.1 | Sulf2 controls generation of glial precursor cells marked by Olig2 expression but distinct from OPCs

In the mouse developing spinal cord, Olig2-expressing (Olig2+) pMN cells start generating OPCs from 12.5 days of development (E12.5). At this initial stage of gliogenesis, *sulf2* is expressed in ventral progenitor cells, including in Olig2+ cells of the pMN domain (Figure 1a). Noticeably, variable levels of *sulf2* mRNA staining were observed in this domain (Figure 1a'), indicating heterogeneous levels of *sulf2* expression within the population of Olig2+ pMN cells. Later on, *sulf2* expression is maintained in ventral progenitor cells but also in few cells streaming away in the spinal parenchyma (Figure 1b). At E14.5, a subset of *sulf2*+ parenchymal cells retains expression of Olig2 (Figure 1b'). Based on these data, Sulf2 appeared to be a reasonable candidate to play a role in OPC development. To test this possibility, we analyzed OPC generation in *sulf2* knocked-out (*sulf2*^{-/-}) embryos using Olig2 together with Sox10, a reliable marker of oligodendroglial cells which is upregulated in Olig2+ pMN cells as soon as they commit to the OPC fate (Kuhlbrodt, Herbarth, Sock, Hermans-Borgmeyer, & Wegner, 1998; Zhou, Wang, & Anderson, 2000). As previously reported (Touahri et al., 2012), we found that, at E12.5 in wild-type embryos, some Olig2+ pMN cells coexpress Sox10 (Figure 1c). Few Olig2+ cells that have already emigrated in the spinal parenchyma were also observed and all of them were found coexpressing Sox10 (Figure 1c). Similar pattern of Olig2 and Sox10 expression was observed in *sulf2*^{-/-} littermates (Figure 1d) and cell counting indicated that the same numbers of Olig2+ pMN cells and Olig2+/Sox10+ parenchymal OPCs have been generated at E12.5 in *sulf2*^{-/-} and wild-type embryos (Figure 1e,f). Therefore, contrasting with previous study (Jiang et al., 2017), our data indicated that Sulf2 is dispensable for initiation of OPC production in the ventral spinal cord. To get further insight on this disparity of results, we next considered the possibility that Sulf2 might impair ongoing OPC production at later developmental stages. We then examined Olig2 and Sox10 expression 1 day later, at E13.5, and, again, found similar patterns of Olig2/Sox10 coexpression in *sulf2*^{-/-} and wild-type littermate embryos (Figure 1g–h',k). We therefore concluded that Sulf2 activity is not required to sustain OPC generation. However, we made at that stage a quite unexpected observation. We found that, in wild-type embryos, while coexpression of Olig2 and Sox10 was detected in most cells streaming away from the pMN domain, expression of Sox10 remained undetectable in a subset of parenchymal Olig2+ cells (Figure 1g–g'', i–i'). These Olig2+/Sox10⁻ cells were predominantly found close to the progenitor zone, suggesting that they had been recently generated. In support of this, we never detected Olig2+/Sox10⁻ cells in the parenchyma at E12.5 (Figure 1c). Strikingly, only few Olig2+/Sox10-

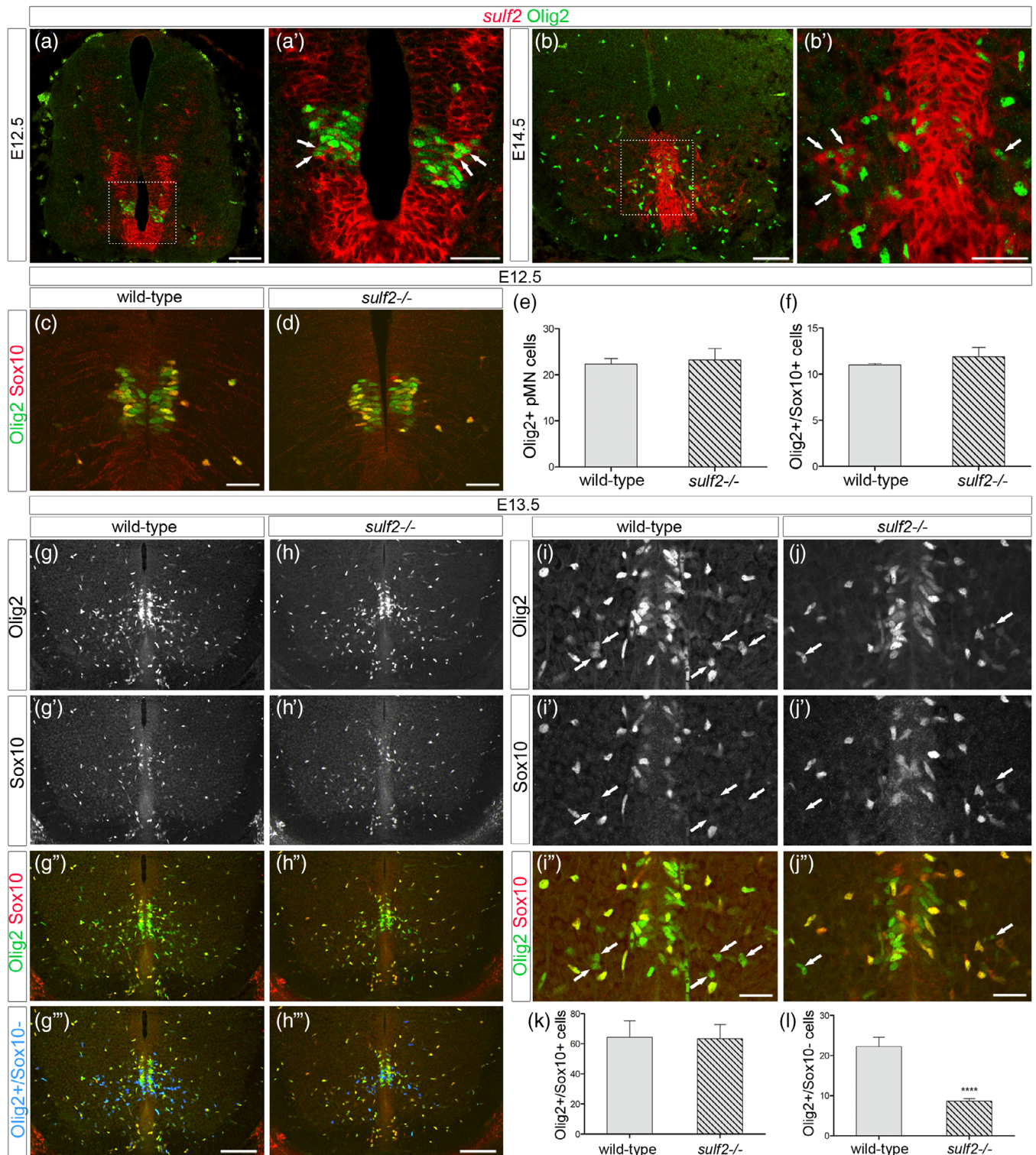


FIGURE 1 *Sulf2* depletion impairs production of Olig2-expressing precursor cells distinct from OPCs. All images show transverse spinal cord sections. (a–b') Combined detection of *sulf2* mRNA (red) and Olig2 (green) at E12.5 (a, a') and E14.5 (b, b'). a' and b' show higher magnification of the areas framed in a and b, respectively. Arrows in a' and b' point to *sulf2*⁺/Olig2⁺ cells. (c, d, g–j'') Double detection of Olig2 (green) and Sox10 (red) at E12.5 (c, d) and E13.5 (g–j'') in wild-type (c, g–g''', i–i'') and *sulf2*^{-/-} (d, h–h''', j–j'') embryos. In g''' and h''', Olig2⁺/Sox10⁻ cells (green only) have been highlighted in blue using Colocalization Finder feature of ImageJ software. Arrows in i–j'' point to Olig2⁺/Sox10⁻ cells. Note reduced number of Olig2⁺/Sox10⁻ cells in the spinal parenchyma of *sulf2*^{-/-} (h'', h''', j'') compared to wild-type (g'', g''', i'') E13.5 embryos. (e–f) Quantification of Olig2⁺ pMN cells (e, n = 4) and Olig2⁺/Sox10⁺ cells (f, n = 4) in E12.5 wild-type and *sulf2*^{-/-} embryos. (k, l) Quantification of Olig2⁺/Sox10⁺ cells (k) and Olig2⁺/Sox10⁻ cells (l) in the E13.5 spinal parenchyma of wild-type (n = 6) and *sulf2*^{-/-} (n = 8) embryos. Data are presented as mean ± SEM (*****p* < .0001). Scale bars = 100 μm in a, b, g–h''' and 50 μm in a', b', c, d, i–j'' [Color figure can be viewed at wileyonlinelibrary.com]

parenchymal cells were detected in *sulf2*^{-/-} littermates (Figure 1h-h'', j-j'') and quantification of these cells indicated that their number was significantly reduced in *sulf2*^{-/-} embryos compared to wild-type littermates (Figure 1l). Deficient generation of Olig2⁺/Sox10⁻ cells

but not of Olig2⁺/Sox10⁺ OPCs was still apparent at fetal stage E18.5, where Olig2⁺/Sox10⁻ cells were still found populating the ventral spinal cord (Figure 2a-f). These results therefore pointed out to a specific function of *sulf2* in controlling generation of

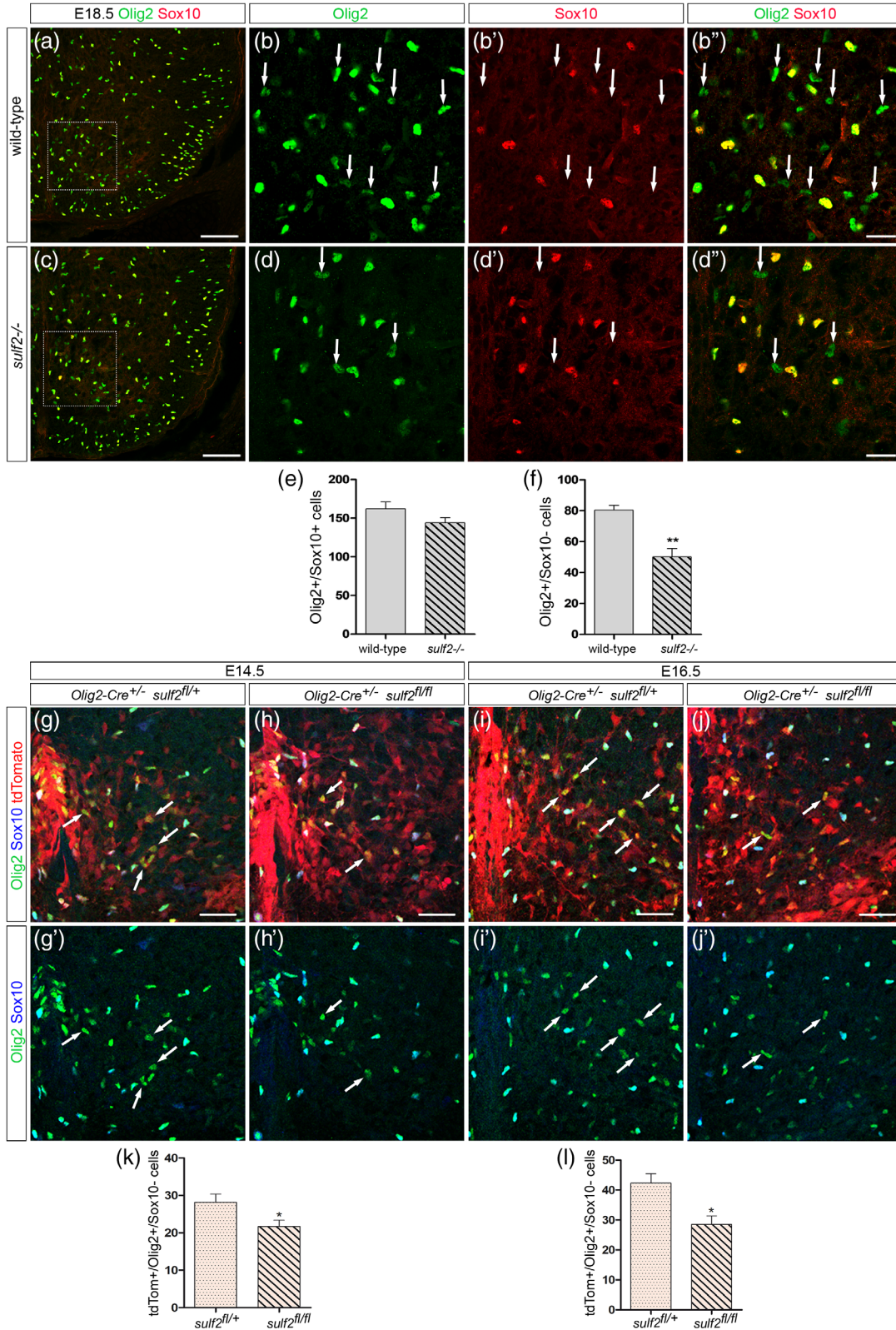


FIGURE 2 Legend on next page.

Olig2+ cells that do not activate Sox10 while populating the spinal parenchyma.

We next asked whether Sulf2 expression specifically in Olig2+ cells is required for proper generation of the Olig2+/Sox10- cell subtype. To test this, we turned to a mouse line that carries a "floxed" allele of *sulf2* (Tran et al., 2012). By breeding *sulf2* "floxed" mice with *olig2* promoter-driven Cre (*Olig2-cre*) knock-in mice (Dessaud et al., 2007), we obtained *sulf2^{fl/+}* and *sulf2^{fl/fl}* littermate embryos on an *Olig2-Cre:Rosa-tdTomato* background. Counting of Olig2+/Sox10- cells was performed in *Olig2-Cre^{+/-}/sulf2^{fl/+}* and *Olig2-Cre^{+/-}; sulf2^{fl/fl}* littermates at E14.5 and E16.5 (Figure 2g-l). We found that, at each stage, the number of Olig2+/Sox10- cells was significantly reduced in *Olig2-Cre^{+/-}; sulf2^{fl/fl}* embryos compared to *Olig2-Cre^{+/-}/sulf2^{fl/+}* littermates (Figure 2k, l). These results therefore support the view that Sulf2 depletion specifically in Olig2+ cells is sufficient to impair generation of Olig2+/Sox10- cells.

Together, our data point out two important issues: (a) two molecularly distinct Olig2+ precursor cell subtypes, namely the Olig2+/Sox10+ OPCs and a second cell population expressing Olig2 but not Sox10, are generated in the ventral spinal cord, (b) Sulf2 expression by Olig2+ cells specifically controls generation of the Olig2+/Sox10- cell subtype.

3.2 | Olig2+/Sox10- cells express astroglial identity genes

The foregoing analysis opened the question of the Olig2+/Sox10- cell identity. Supporting the view that these cells are distinct from OPCs, parenchymal Olig2+/Sox10- cells neither expressed PDGFR α (Figure 3a-b'') nor Olig1 (Figure 3c-d''), both considered as early and specific hallmarks of OPCs in the spinal cord (Meijer et al., 2012; Pringle & Richardson, 1993). We then investigated the possibility that Olig2+/Sox10- cells might be related to the astroglial lineage. For this, we combined immunodetection of Olig2 and in situ localization of *fgfr3*, *aldh1L1*, and *tenascin-C* mRNAs, all reported to mark spinal APs as well as progenitors from which they originate (Cahoy et al., 2008; Karus, Denecke, French-Constant, Wiese, & Faissner, 2011; Pringle et al., 2003). At E13.5, *fgfr3* mRNA was detected in the progenitor zone where its expression domain overlaps the Olig2+ pMN domain (Figure 3e). At this stage, few individual *fgfr3*+ cells were also detected in the spinal parenchyma and, noticeably, most, if not all, of them were positive for the Olig2 staining (Figure 3e), indicating that the first *fgfr3*+ cells to leave the progenitor zone express Olig2. By E15.5, a much greater number of

fgfr3+/Olig2+ cells were found in the ventral parenchyma (Figure 3f). At this stage, *fgfr3*+/Olig2- parenchymal cells were also observed emigrating from ventrally and dorsally located progenitor domains (Figure 3f). Similar results were obtained detecting *aldh1L1* or *tenascin-C* mRNAs and the Olig2 protein (Figure 3g,h). These data therefore revealed the existence of a ventral spinal cord AP subtype that distinguishes itself from others by Olig2 expression.

Due to the setback of combining Sox10 immunostaining with in situ hybridization, we were not able to directly define whether *fgfr3*+/Olig2+ APs match the Olig2+/Sox10- cell population. We therefore turned to *Aldh1L1*-GFP astrocyte-specific reporter mice (Cahoy et al., 2008) and performed immunodetection of the reporter protein together with that of Olig2 and Sox10. We first focused on the progenitor zone of wild-type E12.5 embryos and found the presence of *Aldh1L1*-GFP+/Olig2+ included in the pMN domain (Figure 4a-a''). We also observed at this stage some *Aldh1L1*-GFP+/Olig2+ cells emigrating from the progenitor zone (Figure 4a'). Comparison with the Sox10 staining allowed detecting Olig2+/Sox10+ cells located both in the pMN domain and in the ventral parenchyma (Figure 4a''). Confirming that OPCs do not activate expression of *Aldh1L1*-GFP, Sox10 expression was never detected in *Aldh1L1*-GFP+/Olig2+ cells (Figure 4a'',a'''). These data, by revealing a subtype of Olig2+ pMN cells expressing *Aldh1L1* but not Sox10 at E12.5, bring direct evidence for generation of glial precursor cells displaying an AP identity in the pMN domain. We next asked whether generation of *Aldh1L1*-GFP+/Olig2+/Sox10- cells is impaired by *sulf2* loss-of-function. At E13.5 in wild-type embryos, *Aldh1L1*-GFP+/Olig2+/Sox10- cells were still detected in the ventral progenitor zone and were also found emigrating in the mantle layer (Figure 4b-b''). Although *Aldh1L1*-GFP+/Olig2+/Sox10- cells were also detected in *sulf2* mutant embryos (Figure 4c-c''), cell counting indicated that they were reduced in number in these embryos compared to wild-type littermates (Figure 4e) and no significant difference was found in the number of *Aldh1L1*-GFP/Olig2+/Sox10+ cells between wild-type and *sulf2*-/- embryos (Figure 4d). Together, these data add further support to the view that Sulf2 plays a role in triggering generation of Olig2+ APs from progenitor cells of the pMN domain.

To learn more about the Olig2+ AP subtype, we next performed immunostaining using antibodies specific for Nkx6.1, expressed in APs originating from ventral progenitors, and for NFIA and Zeb1, two transcription factors broadly expressed in newly generated spinal APs (Deneen et al., 2006; Ohayon et al., 2016; Zhao et al., 2014). We found that essentially all Olig2+/Sox10- cells coexpress these proteins

FIGURE 2 Deficient production of Olig2+/Sox10- cells is detectable at late embryonic stage and in CreLox model deleting *sulf2* specifically in Olig2+ neural progenitors. All images show transverse sections of hemi-ventral spinal cord. (a-d'') Double detection of Olig2 (green) and Sox10 (red) at E18.5 in wild-type (a, b-b'') and *sulf2*-/- (c, d-d'') embryos. b-b'' and d-d'' show higher magnification of the areas framed in a and c, respectively. Arrows in b-b'' and d-d'' point to Olig2+/Sox10- cells. (E-F) Quantification of Olig2+/Sox10+ cells (e) and Olig2+/Sox10- cells (f) in the E18.5 spinal parenchyma of wild-type (n = 5) and *sulf2*-/- (n = 5) embryos. (g-j') Detection of Olig2 (green), Sox10 (blue) and tdTomato (red) at E14.5 (g, h) and E16.5 (i, j) in *Olig2-Cre^{+/-}/sulf2^{fl/+}* (g, i) and *Olig2-Cre^{+/-}; sulf2^{fl/fl}* (h, j) embryos. g'-j' show double staining of Olig2 and Sox10 corresponding to g-j. Note high level of tdTomato expression reflecting efficient recombinase activity of the Cre protein in the ventral spinal cord. (k, l) Quantification of Olig2+/Sox10- cells in the spinal parenchyma of *Olig2-Cre^{+/-}/sulf2^{fl/+}* and *Olig2-Cre^{+/-}; sulf2^{fl/fl}* embryos at E14.5 (k, n = 5 for each genotype) and at E16.5 (l, n = 5 for each genotype). Data are presented as mean \pm SEM (**p < .01, *p < .05). Scale bars = 100 μ m in a, c and g-j' and 25 μ m in b-b'', d-d'' [Color figure can be viewed at wileyonlinelibrary.com]

at E14.5 (Figure 5), indicating that they share the same basic properties as previously identified ventral APs.

Together, these data reveal the existence of a spinal AP subtype that emerge from Olig2-expressing progenitor cells and maintain Olig2 expression as they populate the ventral spinal parenchyma. For convenience, we refer to this sub-population henceforth as Olig2+ APs.

3.3 | Olig2+ APs maintain expression of Olig2 while activating astrocyte differentiation genes

We next examined whether, as previously reported for cortical white matter APs (Cai et al., 2007; Marshall, Novitch, & Goldman, 2005), expression of Olig2 in ventral spinal cord APs reflects an immature

stage of astrocytogenesis. Specific markers for different stages of AP maturation are not available. However, acquisition of mature astrocyte identity in the spinal cord can be followed according to the previously reported stepwise process of their maturation (Tien et al., 2012). This process progresses through different stages: a proliferating intermediate AP stage, during which parenchymal APs remain proliferative (E14.5 to P3); a maturing postnatal astrocyte stage (from P5) in which APs no more proliferate and an adult astrocyte status. We therefore assessed Olig2 and Sox10 expression at early (P2) and late (P7) postnatal stages as well as in adult spinal cord, postulating that, if Olig2 expression in Olig2+ APs is downregulated as these cells undergo terminal differentiation, the population of Olig2+/Sox10- cells should progressively disappear. Olig2+/Sox10- cells were still

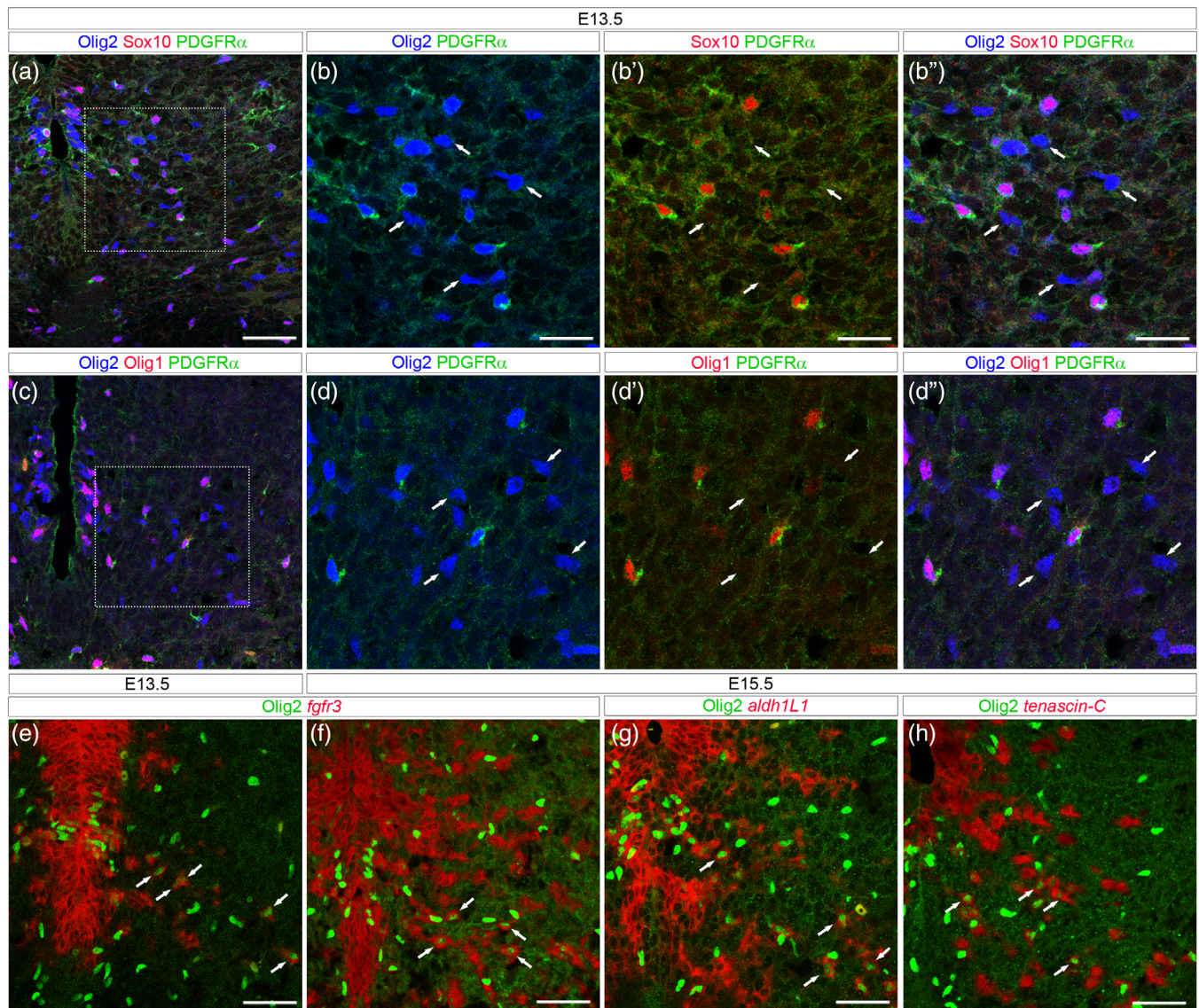


FIGURE 3 Olig2+/Sox10- cells express AP but not OPC markers. All images show transverse spinal cord sections. (a-d'') Combined detection of Olig2 (blue), PDGFRα (green) and Sox10 (a, b-b'', red) or Olig1 (c, d-d'', red) viewed on E13.5 hemi-ventral spinal cord. b-b'' and d-d'' show higher magnification of the area framed in a and c, respectively. Arrows point to Olig2+ cells that are not stained with the OPC markers. (e-h) Combined detection of Olig2 (green) and mRNAs (red) encoding for *fgfr3* (e, f), *aldh1L1* (g) and *tenascin-C* (h) viewed on E13.5 (e) and E15.5 (f-h) hemi-ventral spinal cords. Note, in all panels, the presence of Olig2+ cells stained with mRNA probes (arrows). Scale bars = 50 μm in a, c, e-h and 25 μm in b-b'', d-d'' [Color figure can be viewed at wileyonlinelibrary.com]

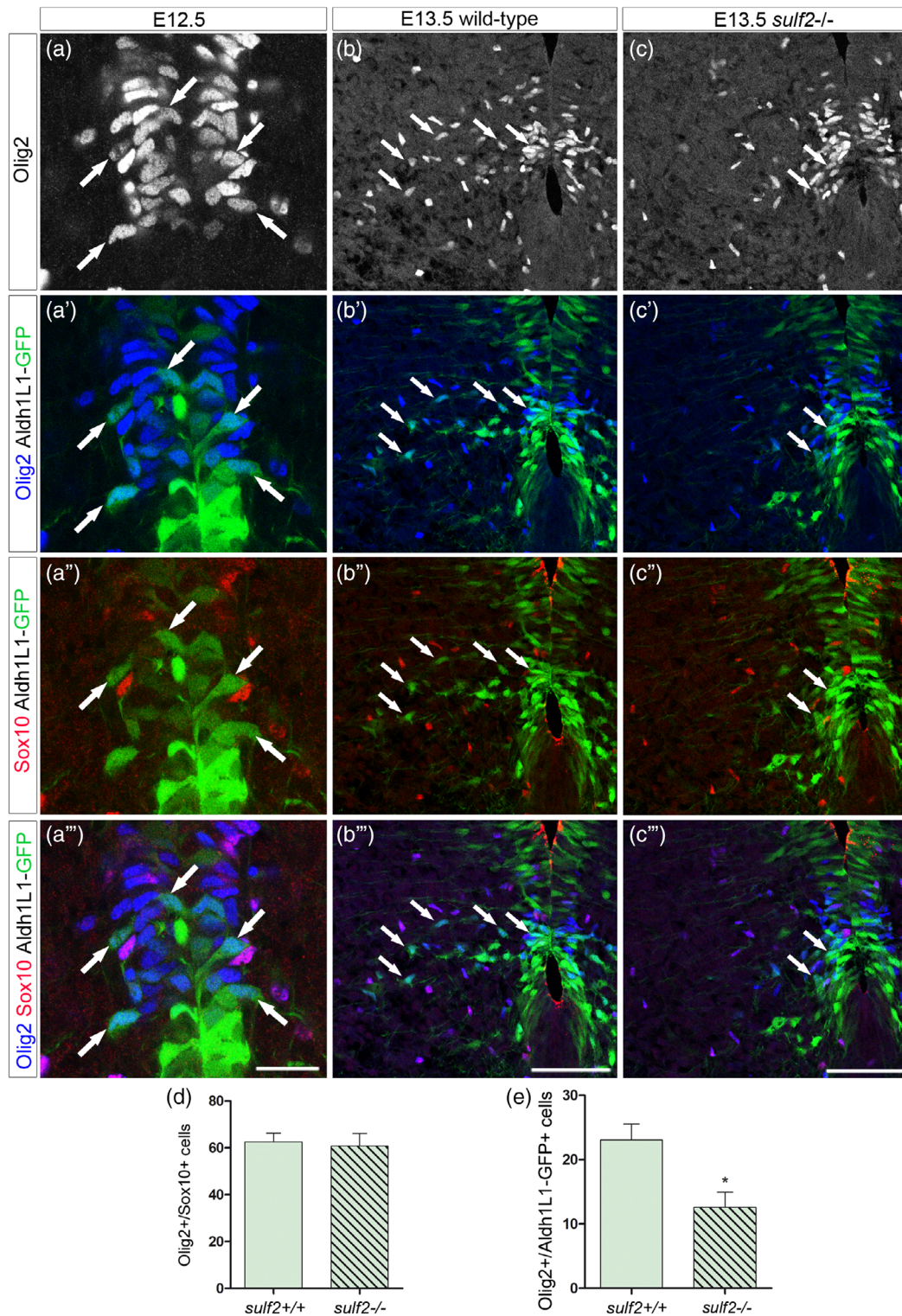


FIGURE 4 *Sulf2* depletion impairs production of Aldh1L1-GFP⁺/Olig2⁺ cells originating from the pMN domain. All images show transverse spinal cord sections. (a–c'') Combined detection of Olig2 (blue), Sox10 (red), and GFP (green) on Aldh1L1-GFP transgenic embryos on a *sulf2* wild-type background at E12.5 (a–a'') and E13.5 (b–b'') and on *sulf2*^{-/-} background at E13.5 (c–c''). Vertical sets present successively Olig2 staining, Olig2 and Aldh1L1-GFP staining, Sox10 and Aldh1L1-GFP staining and the merged image. Arrows in all panels point to Olig2⁺/Sox10⁻ cells. a–a'' show high magnification of the ventral progenitor zone. Note the presence of GFP⁺/Olig2⁺/Sox10⁻ cells both in the progenitor zone (Olig2⁺ pMN domain) and in the adjacent spinal parenchyma. (d) Quantification of Olig2⁺/Sox10⁺ cells in E13.5 wild-type and *sulf2*^{-/-} embryos (*n* = 5 for each genotype). (e) Quantification of Aldh1L1-GFP⁺/Olig2⁺/Sox10⁻ cells in E13.5 wild-type and *sulf2*^{-/-} embryos (*n* = 5 for each genotype). Data are presented as mean ± SEM (**p* < .05). Scale bars = 25 μm in a–a'' and 75 μm in b–c'' [Color figure can be viewed at wileyonlinelibrary.com]

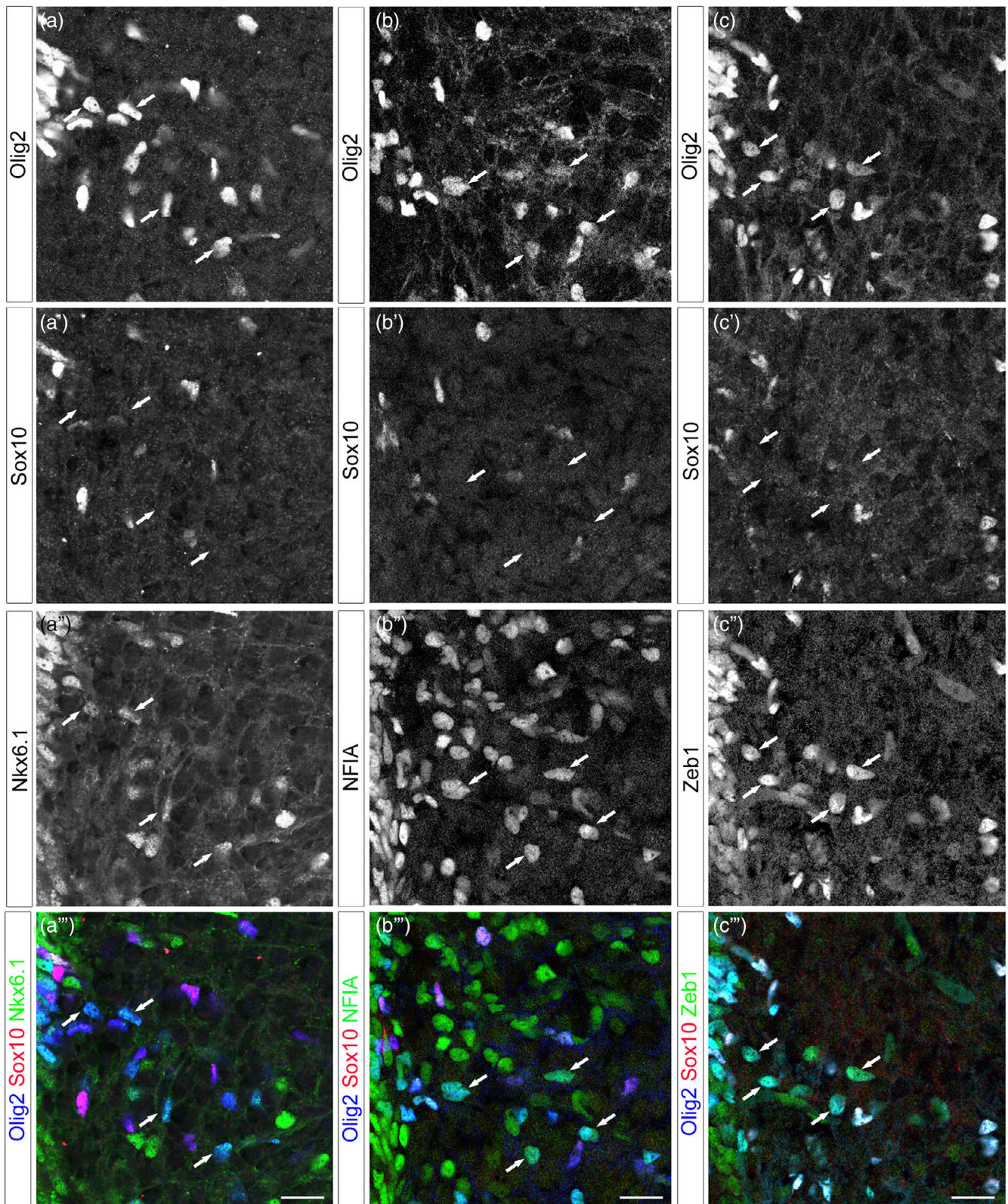


FIGURE 5 Olig2⁺/Sox10⁻ cells coexpress a set of AP nuclear proteins as they populate the ventral spinal parenchyma. All images show transverse sections of hemi-ventral spinal cord, ventral progenitor zone is on the upper left. (a–c^{'''}) Combined detection of Olig2 (blue), Sox10 (red), and Nkx6.1 (a^{''}–a^{'''}, green), NFIA (b^{''}–b^{'''}, green) or Zeb1 (c^{''}–c^{'''}, green) at E14.5. Vertical sets present successively Olig2 staining, Sox10 staining followed by astrocytic marker staining and the corresponding merged image. Arrows point to Olig2⁺/Sox10⁻ cells positive for the astrocytic markers. Scale bars = 50 μ m [Color figure can be viewed at wileyonlinelibrary.com]

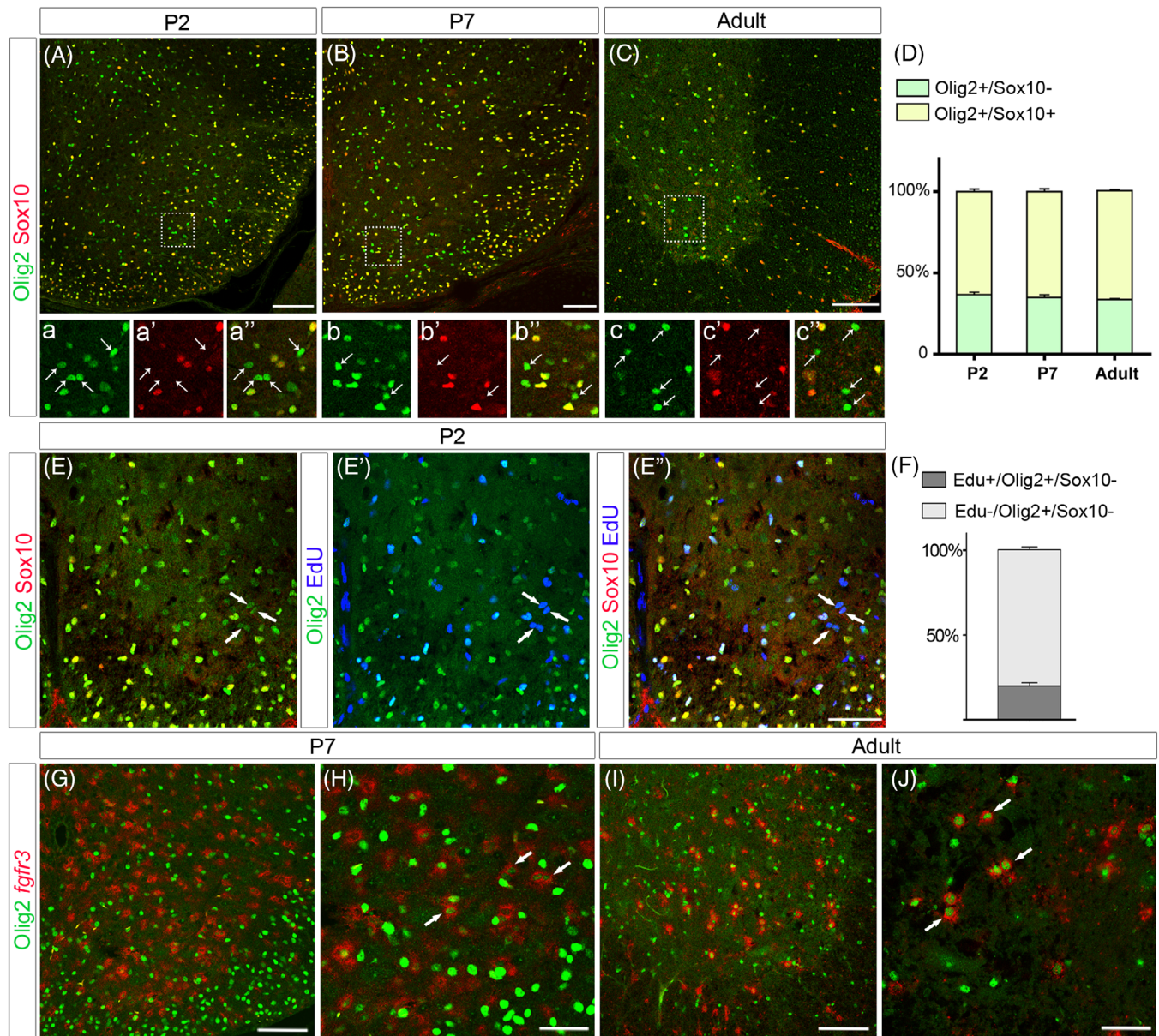


FIGURE 6 Olig2+/Sox10⁻ cells are maintained at postnatal and at adult stages

All images show transverse sections of hemi-ventral spinal cord. (A–c'') Double detection of Olig2 (green) and Sox10 (red) at P2 (A, a–a''), P7 (B, b–b''), and adult (C, c–c'') stages. Images a–a'', b–b'', and c–c'' show higher magnification of the areas framed in A, B, and C, respectively and horizontal sets present successively Olig2 staining, Sox10 staining and the merged image. Note the presence of Olig2+/Sox10⁻ cells (arrows) at all stages. (D) Proportion of Sox10⁻ and Sox10⁺ cells on the Olig2⁺ cell population in the ventral spinal cord at P2 ($n = 5$), P7 ($n = 5$) and at adult stage ($n = 5$). (E–E'') Combined detection of Olig2 (green), Sox10 (red) and EdU (blue) at P2. Images E, E', and E'' show successively Olig2/Sox10 staining, Olig2/EdU staining, and the merged image. Arrows point to Olig2+/Sox10⁻ cells positive for EdU. (F) Proportion of EdU⁺ cells on the Olig2+/Sox10⁻ cell population at P2 ($n = 4$). (G–J) Double detection of Olig2 (green) and *fgfr3* mRNA (red) viewed on ventral spinal cord hemi-section at P7 (G, H) and at adult stage (I, J). H and J are high magnifications of the ventral spinal cord in which arrows point to Olig2+/*fgfr3*⁺ cells. Data are presented as mean \pm SEM. Scale bars = 100 μ m in A–E'', G, I and 50 μ m in H and J [Color figure can be viewed at wileyonlinelibrary.com]

detected in the ventral spinal cord at postnatal and adult stages (Figure 6A–C) and no significant difference was found at each stage in their rates relative to the Olig2+/Sox10⁺ oligodendroglial cell population (Figure 6D), indicating that the Olig2+/Sox10⁻ ventral spinal cell population persists at stages of astrocyte maturation. EdU injection over the period of P0 to P2 indicated that 20% of these cells incorporated EdU (Figure 6E–E''), corresponding to the expected proliferation

profile for APs at early postnatal stages (Tien et al., 2012). We also found that, at postnatal and adult stages, Olig2 still showed colocalization with the AP marker *fgfr3* (Figure 6G–J), indicating that Olig2 expression is retained in astroglial cells until adult stage.

To further characterize the Olig2⁺ astroglial cell population, we analyzed expression of a set of glial cell markers in postnatal (P7) and adult Aldh1L1-GFP spinal cords. We found extensive coexpression of

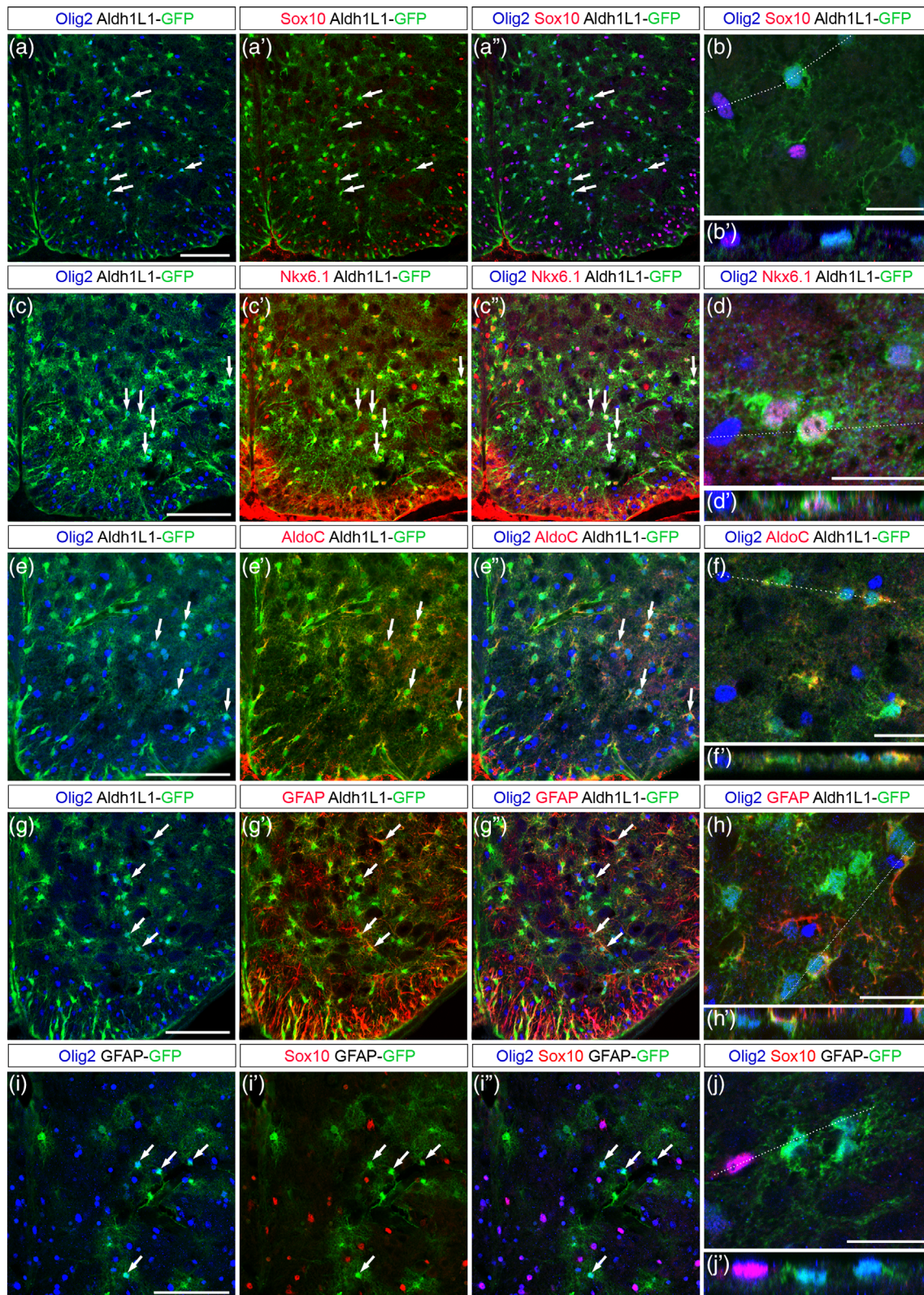


FIGURE 7 Olig2⁺ APs retain expression of Olig2 as they differentiate in the P7 ventral spinal cord. Images show transverse sections of P7 hemi-ventral spinal cord. (a–j') Combined detection of Olig2 (blue), Sox10 (a'–b', i'–j', red), Nkx6.1 (c'–d', red), AldoC (e'–f', red) or GFAP (g'–h', red) in Aldh1L1-GFP (a–h', green) and GFAP-GFP (i–j', green) transgenic individuals. Horizontal sets present successively Olig2 and GFP staining, Sox10, Nkx6.1, AldoC or GFAP and GFP staining (prime) and the merged image (double prime). Arrows point to Olig2⁺ cells positive for the astrocytic markers. Panels b, d, f, h and j show higher magnification of the ventral grey matter and underneath prime panels show images in the Z-plane, corresponding to the dashed line drawn in the X/Y plane above. Scale bars = 100 μm in a–a', c–c', e–e', g–g', and i–i' and 25 μm in b, d, f, h, and j [Color figure can be viewed at wileyonlinelibrary.com]

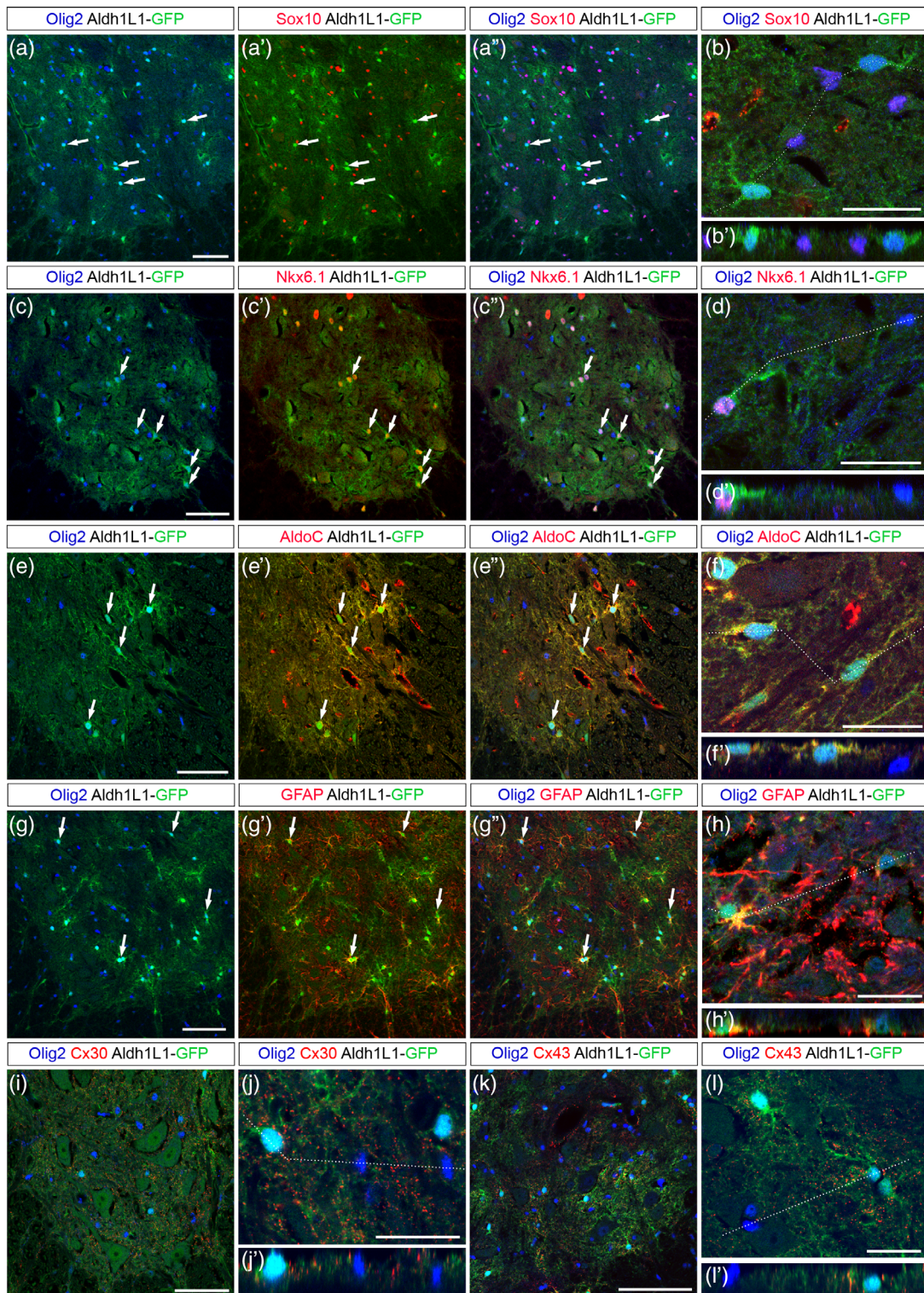


FIGURE 8 Olig2⁺ astrocytes are maintained in the grey matter of the adult spinal cord. Images show transverse sections of adult hemi-ventral spinal cord. (a–h') Combined detection of Olig2 (blue) and Sox10 (a'–b', red), Nkx6.1 (c'–d', red), AldoC (e'–f', red) and GFAP (g'–h', red) in Aldh1L1-GFP (green) transgenic individuals. Horizontal sets present successively Olig2 and GFP staining, Sox10, Nkx6.1, AldoC or GFAP and GFP staining (prime) and the merged image (double prime). Arrows point to Olig2⁺ cells positive for the astrocytic markers. Panels b, d, f, and h show higher magnification of the ventral grey matter and underneath prime panels show images in the Z-plane, corresponding to the dashed line drawn in the X/Y plane above. (i–l') Combined detection of Olig2 (blue), GFP (green), and Cx30 (i–j') or Cx43 (k–l') on Aldh1L1-GFP adult spinal cord. Panels j and l show higher magnification of the ventral grey matter and underneath prime panels show images in the Z-plane, corresponding to the dashed line drawn in the X/Y plane above. Scale bars = 100 μ m in a–a' and K, 50 μ m in c–c', e–e', g–g' and i–i' and 25 μ m in b, d, f, h, j, and l [Color figure can be viewed at wileyonlinelibrary.com]

Aldh1L1-GFP and Olig2 but not Sox10 at P7 (Figure 7a–b') and at adult stage (Figure 8a–b'). Supporting the view that they originate from ventral progenitors, Aldh1L1-GFP+/Olig2+ cells were all found coexpressing Nkx6.1 (Figures 7c–d' and 8c–d'). We next examined expression of the astrocytic marker AldoC and found that a fraction of ventral Aldh1L1-GFP+/AldoC+ cells indeed express Olig2 at both stages (Figures 7e–f' and 8e–f'). We then analyzed expression of the astrocyte maturation marker GFAP and also found Aldh1L1-GFP+/Olig2+ cells expressing GFAP in P7 (Figure 7g–h') and adult individuals (Figure 8g–h'). To confirm this, we analyzed expression Olig2 and Sox10 in GFAP-GFP transgenic mice in which expression of the reporter allows complete staining of astrocyte cell bodies (Nolte et al., 2001). In these mice, GFAP-GFP+ cells coexpressing Olig2 were also detected in the ventral spinal parenchyma at P7 (Figure 7i–j'). Finally, we examined expression of the connexin proteins Cx43 and Cx30, known to be differentially expressed in astrocytes of the adult rodent spinal cord (Orthmann-Murphy, Abrams, & Scherer, 2008). Immunostainings of Cx43 and Cx30 together with that of Olig2 were performed on sections of adult Aldh1L1-GFP spinal cords (Figure 8i–l'). Characteristic punctate immunoreactivity was observed for both Cx43 and Cx30 on Olig2+/Aldh1L1-GFP+ cells whose soma and processes can be detected by the endogenous fluorescence of GFP (Figure 8j,j' and l,l').

Together, these data, showing that Olig2 expression is retained at postnatal and adult stages in cells expressing the AP markers *fgfr3*, Aldh1L1 and Nkx6.1 but also in cells that activate expression of functionally relevant astrocyte differentiation markers AldoC, GFAP, Cx43, and Cx30 support the view that Olig2+ APs maintain Olig2 expression as they mature in the ventral spinal cord.

3.4 | Sulf2 depletion while impairing the first wave of AP production does not cause major spinal cord AP deficit

Sulf2 expression is not restricted to the pMN domain, but extends ventrally and dorsally in progenitor domains known to generate V1 to V3 APs (see Figure 1a,b). Analysis of *sulf2* expression over spinal cord development further revealed *sulf2*+ parenchymal cells streaming away at all levels of the ventral progenitor zone (Figure 9a–c), within a pattern very suggestive of *sulf2* expression being maintained in most, if not all, ventral spinal cord APs. Confirming the AP identity of parenchymal *sulf2*+ cells, we found that these cells coexpress *fgfr3* but not *sox10* as they leave the progenitor zone (Figure 9d,e). We next logically asked whether Sulf2 might have a general influence on AP generation. To investigate this question, we compared the time course of *fgfr3* expression in wild-type and *sulf2*^{-/-} embryos. At E13.5, when the first wave of AP production became discernible in wild-type embryos (Figure 10a), only very few *fgfr3*+ cells were found emigrating from the progenitor zone in *sulf2*^{-/-} embryos (Figure 10e) and cell quantification confirmed defective production of *fgfr3*+ cells in *sulf2*^{-/-} embryos compared to wild-type littermates (Figure 10i). Thus, as expected since the first APs to be generated correspond to the Olig2+ AP subtype (see Figure 3), Sulf2 depletion causes defective AP production at initiation of astrogenesis. At E14.5 and E15.5, although cell counting still indicated a decrease in the number of ventral *fgfr3*+ cells in mutant embryos (Figure 10j,k), numerous *fgfr3*+ individual cells were found populating the spinal parenchyma both in wild-type (Figure 10b,c) and *sulf2*^{-/-} embryos (Figure 10f,g). At E18.5, larger numbers of *fgfr3*+ cells were found populating the spinal cord parenchyma of wild-type (Figure 10d) and *sulf2*^{-/-} embryos

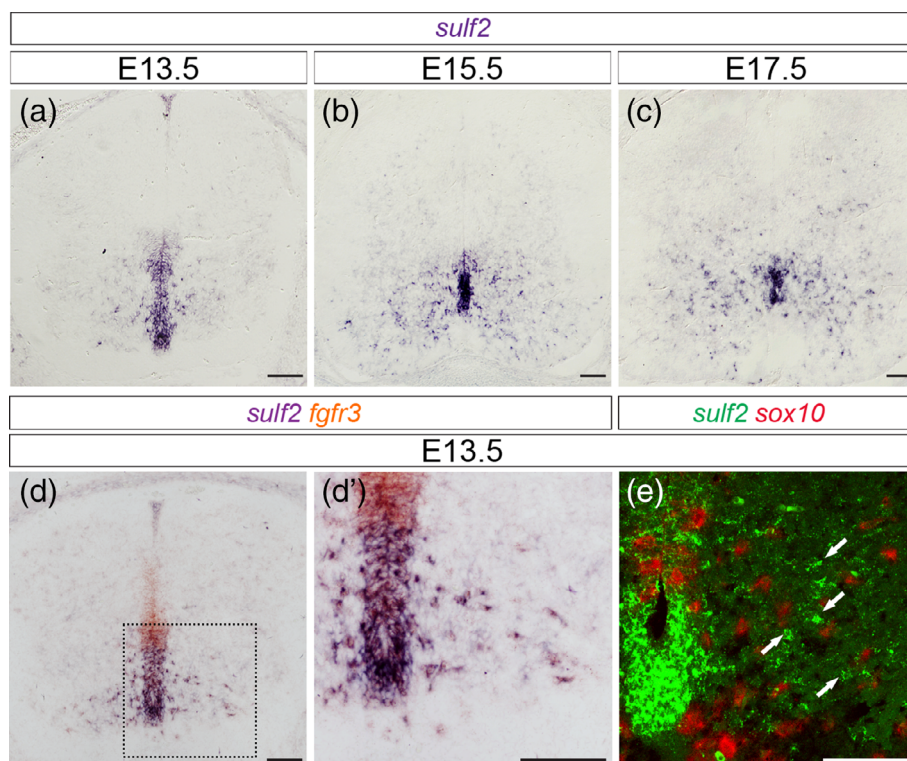


FIGURE 9 Sulf2 is broadly expressed in ventral APs as they populate the spinal parenchyma. All images show transverse spinal cord sections. (a–c) Temporal expression profile of *sulf2* mRNA at E13.5 (a), E15.5 (b), and E17.5 (c). (d, d') Combined detection of *sulf2* (brown) and *fgfr3* (purple) mRNAs. d' shows higher magnification of the area framed in d. (e) Combined detection at confocal resolution of *sulf2* (green) and *sox10* (red) mRNAs in hemi-ventral spinal cord at E13.5. Scale bars = 100 μm [Color figure can be viewed at wileyonlinelibrary.com]

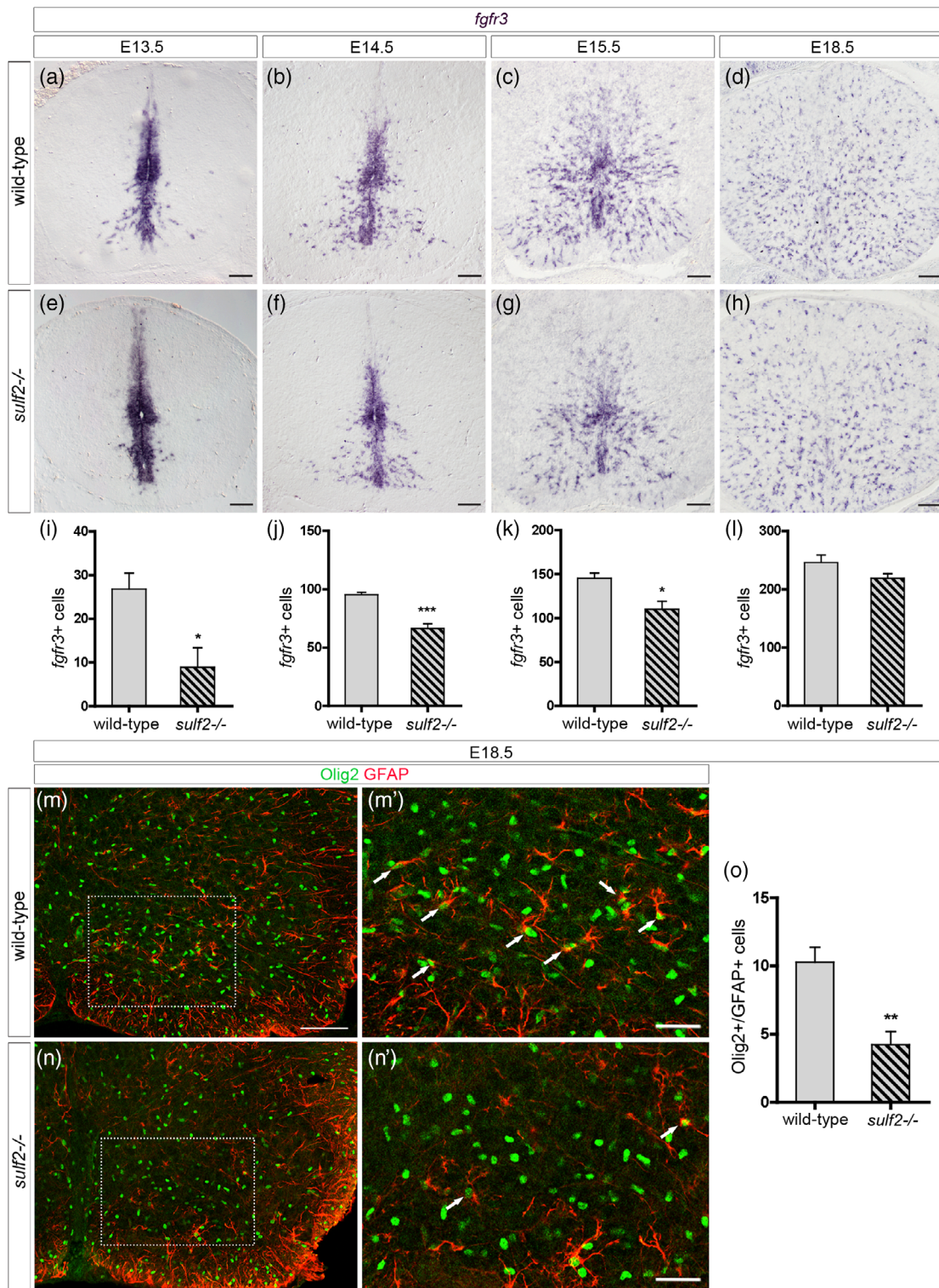


FIGURE 10 Sulf2 depletion impairs early wave of AP production but does not cause major defect of astrocytogenesis. All images show transverse spinal cord sections. (a–h) Detection of parenchymal cells expressing *fgfr3* mRNA in wild-type (a–d) and *sulf2*^{-/-} (e–h) embryos at E13.5 (a, e), E14.5 (b, f), E15.5 (c, g), and E18.5 (d, h). (i–l) Quantification of *fgfr3*⁺ parenchymal cells in wild-type and *sulf2*^{-/-} embryos at E13.5 (i; wild-type $n = 7$; *sulf2*^{-/-} $n = 5$), E14.5 (j; wild-type $n = 6$; *sulf2*^{-/-} $n = 4$), E15.5 (k; $n = 5$ for each genotype) and E18.5 (l; $n = 5$ for each genotype). (m–n') Double detection of Olig2 (green) and GFAP (red) in wild-type (m, m') and *sulf2*^{-/-} (n, n') spinal cords at E18.5. m' and n' show higher magnification of the area framed in m and n, respectively. Arrows in m' and n' point to Olig2⁺/GFAP⁺ cells. (o) Quantification of Olig2⁺/GFAP⁺ cells in the ventral spinal cord of E18.5 wild-type and *sulf2*^{-/-} embryos ($n = 5$ for each genotype). Data are presented as mean \pm SEM (*** $p < .001$, ** $p < .01$, and * $p < .05$). Scale bars = 100 μ m in a–h, m, n and 50 μ m in m', n' [Color figure can be viewed at wileyonlinelibrary.com]

(Figure 10h) and cell counting indicated a downward trend, although not significant, of their number in *sulf2*^{-/-} compared to wild-type individuals (Figure 10l), indicating no gross effect of *Sulf2* depletion on astrocyte development. To distinguish Olig2⁺ APs among the overall population, we next combined Olig2 and GFAP detection in E18.5 wild-type and *sulf2*^{-/-} embryos. As expected, GFAP⁺/Olig2⁺ cells were detected in the ventral spinal parenchyma of wild-type embryos (Figure 10m–m'). Only few GFAP⁺/Olig2⁺ cells were found in *sulf2*^{-/-} embryos (Figure 10n–n') and cell counting confirmed that their number was significantly reduced compared to wild-type littermates (Figure 10o), thus confirming that proper generation of this astrocyte subtype depends on *Sulf2* activity.

Therefore, *Sulf2* depletion, while affecting the first wave of AP production, did not cause a massive defect in the generation of ventral spinal cord APs. These data not only reinforce the view that Olig2⁺ astrocytes depend on *Sulf2* for their development but also highlight the role of *Sulf2* for proper generation of this particular AP subtype.

4 | DISCUSSION

Astrocytes are currently considered to be a remarkably heterogeneous population of cells exhibiting highly diverse functional properties that can impact their influence on neuronal transmission. However, although functional heterogeneity of astrocytes is a well-established concept, how this diversity is generated still remains elusive. In particular, the question remains whether patterning transcription factors contribute to generate stable molecular and functional diversity in astrocytes, as they do in neurons. In the present work, by addressing the role of *Sulf2* in the mouse embryonic spinal cord, we highlight a specific function for this enzyme in controlling production of a specific AP subtype, which, remarkably, expresses Olig2 at all stages of its development. We therefore characterized astrocytes displaying an "Olig2 identity" from initial stage of their generation to terminal differentiation in the ventral spinal cord and identified a specific player of their generation.

Our work reveals a previously undefined heterogeneity within the population of Olig2⁺ glial precursor cells generated in the early gliogenic spinal cord. So far, although pMN cells are recognized to generate some astroglial cells (Masahira et al., 2006; Tsai et al., 2012), the nature of their precursor cells in the spinal cord parenchyma was unknown. Thus, OPCs were the only pMN-derived glial precursor cells to have been characterized. Typical OPC molecular identity relies on expression of Olig2 together with Sox10, Olig1, and PDGFR α , a set of genes activated as soon as pMN cells commit to the OPC fate (Bergles & Richardson, 2015). We identified a subtype of Olig2⁺ cells that do not activate this OPC program but, instead, adopt AP molecular features, activating expression of *fgfr3*, *Aldh1L1*, *TenascinC*, and *Nkx6.1*, adopting later on definitive astrocyte identity with expression of structural and functional proteins such as AldoC, GFAP, Cx43 and Cx30.

Noticeably, OPCs (Olig2⁺/Sox10⁺) and APs (Olig2⁺/Aldh1L1⁺) are already distinguishable within the pMN domain, indicating that they segregate early, before leaving the progenitor zone. We did not

detect real distinct sub-domains within the pMN domain, where the two Olig2⁺ cell subtypes appeared instead intermingled. This therefore questions the model of spatial segregation into distinct progenitor cell domains for glial-cell subtype specification in the developing spinal cord. Several types of glial restricted precursor cells that can generate astrocytes and oligodendrocytes (O-A precursor cells) have been identified in the past, including Glial-Restricted Precursor cell (GRP) and O-2A cells (Liu & Rao, 2004). However, their existence in vivo has been the subject of debate (Rowitch & Kriegstein, 2010). Our results showing that OPCs and APs develop in the same region of the neural tube are consistent with the O-A precursor cell model, opening the possibility that Olig2⁺ progenitor cells of the pMN domain might share common features with these bipotent glial precursor cells at gliogenic stages. However, the possibility that Olig2⁺ cells are heterogeneous and that OPC and AP fate-restricted Olig2⁺ progenitors are included in the pMN domain cannot be excluded.

A previous study by Jiang and collaborators (Jiang et al., 2017) reported that *Sulf2* depletion caused deficient production of OPCs at the initial stage of gliogenesis, that is, E12.5. Here we show that lack of *Sulf2* leads to defective Olig2⁺ AP generation but has no effect on OPC generation during all development, from E12.5 to E18.5. At first, differences in mouse models and/or markers used to identify OPCs could possibly account for these differences. However, both mouse lines from Nagamine and collaborators (Nagamine et al., 2012) in the study of Jiang and collaborators and from Ai and collaborators (Ai et al., 2007) in the present study, should be functionally similar inasmuch as they carry deletions in the region encoding the catalytic site of the enzyme. Also, cells expressing PDGFR α (as in the study of Jiang et al., 2017) or Olig2/Sox10 (as in our present work) are recognized as a single cell population in the embryonic ventral spinal cord (Finzsch, Stolt, Lommes, & Wegner, 2008; Zhou et al., 2000). Therefore, there is currently no evident explanation for this discrepancy. Nevertheless, the effect of the lack of *Sulf2* on Olig2⁺ AP generation highlights the important role of *Sulf2* in glial subtype development.

How *Sulf2* participates in the control of Olig2⁺ AP generation remains to be established. *Sulf2*, together with *Sulf1*, are recognized as critical regulators of heparan sulfate (HS) activities through their ability to catalyze specific 6-O-desulfation of the polysaccharide (El Masri et al., 2017). HS, found at the cell surface and in the extracellular matrix, interact with many signaling cues and a major determinant of specificity and affinity of HS-ligand interactions is 6-O-sulfation. Then, Sulf proteins by post-synthetically modulating levels of 6-O-sulfation regulate HS binding properties toward numerous ligands important in development, including Shh, FGFs, Wnt, and BMPs. HS on heparan sulfate proteoglycans (HSPGs) are known to modulate signaling activities in many different ways: they can regulate ligand secretion, processing, and access to receptors but HSPGs can also act as receptors or co-receptors (Rosen & Lemjabbar-Alaoui, 2010). We know from our previous work that *Sulf1*, expressed by Shh secreting cells of the medial and lateral floor plate cells but not by the Olig2⁺ pMN responsive cells, contributes to induce OPC generation by controlling delivery of inductive signal provided by Shh (Al Oustah et al., 2014; Touahri et al., 2012). In contrast to *Sulf1*, *Sulf2* is

expressed by Olig2+ progenitor cells of the pMN domain, opening the possibility that *Sulf2* might control gliogenesis acting cell autonomously on these cells. This is supported by our data showing that inactivation of *Sulf2* specifically in Olig2-expressing cells is sufficient to impair generation of Olig2+ APs. Noticeably, we found heterogeneity in levels of *sulf2* expression among pMN cells. Therefore, an attractive hypothesis could be that high levels of *Sulf2* expression in a subset of Olig2+ progenitor cells favor reception of astroglial inductive signal. A set of signaling factors, including members of the interleukin-6 family of cytokines such as LIF and CNTF, which activate the JAK-STAT pathway as well as BMP-Smad and Notch signaling have been shown to promote astrocyte differentiation from neural stem/progenitor cells (Gallo & Deneen, 2014; Kanski, van Strien, van Tijn, & Hol, 2014). However, effects of these factors on astrocytogenesis have primarily been studied by their ability to induce GFAP expression and we now know that the specification of APs from neural progenitors occurs before GFAP induction during development. Thus, whether these factors contribute to actively instruct neural precursor cells to follow an astroglial fate and, thereby, whether they might correspond to signal regulated by *Sulf2*, remains an open question.

An important aspect of our study is the characterization of ventral spinal cord astrocytes that maintain expression of Olig2 until they reach their mature stage. Previous studies already noted the presence of GFAP+ astrocytes coexpressing Olig2 in the grey matter of the adult mouse spinal cord (Barnabé-Heider et al., 2010; Guo et al., 2011). Even if some Olig2+ astrocytes were occasionally observed in the white matter, we also found that most Olig2+ astrocytes are located in the grey matter, supporting the view they are related to protoplasmic astrocytes. Similarly, subpopulation of glial cells co-expressing astrocytic genes and Olig2 have been reported to populate the thalamus (Griemsmann et al., 2015), indicating that Olig2 expression is also maintained in at least subtypes of astrocytes of the adult brain. Therefore, our work, by uncovering production of Olig2+ APs at initial stages of gliogenesis, sheds light on the developmental origin of spinal cord Olig2+ astrocytes. The most striking aspect is that ventral spinal Olig2+ APs maintain expression of Olig2 as they acquire a mature astrocytic identity. It is therefore obvious that, at least for this particular astrocyte subtype, Olig2 does not behave as a repressor of astrocytogenesis. Nonetheless, this observation raises the question whether expression of Olig2 confers specific functional properties to these astrocytes. During the past decade, evidence has accumulated that astrocytes represent remarkably heterogeneous cells that differ in their morphology, developmental origin, gene expression profile, physiological properties, function, and response to injury and disease (Adams & Gallo, 2018; Ben Haim & Rowitch, 2017). Our study, by revealing the time of birth and molecular identity of pMN-derived astrocytes as well as a key regulator of their production during development, therefore represents an important advance in clarifying astrocyte heterogeneity in the spinal cord.

ACKNOWLEDGMENTS

We especially thank X. Ai, N. Rouach, H. Kettenmann and B. Novitsch for their generous sharing of *Sulf2* mutant, *Aldh1L1*-GFP, GFAP-GFP,

and Olig2-Cre mice, respectively. We acknowledge B. Guiard for the gift anti-Connexin antibodies and A. Pattyn for providing valuable reagents and for critical reading of the manuscript. We thank the ABC facility and ANEXPLO for housing mice and the Toulouse Regional Imaging Platform (TRI) for technical assistance in confocal microscopy. We acknowledge the Developmental Studies Hybridoma Bank, developed under the auspice of NICHD and maintained by the University of Iowa, Department of Biological Sciences, Iowa City, IA, for supplying monoclonal antibodies. Work in C.S.' lab was supported by grants from ANR, ARC, ARSEP, CNRS, and University of Toulouse. D. O. was supported by grants from ARSEP and ARC.

ORCID

Cathy Soula  <https://orcid.org/0000-0002-9027-9994>

REFERENCES

- Adams, K. L., & Gallo, V. (2018). The diversity and disparity of the glial scar. *Nature Neuroscience*, 21(1), 9–15. <https://doi.org/10.1038/s41593-017-0033-9>
- Ai, X., Kitazawa, T., Do, A. T., Kusche-Gullberg, M., Labosky, P. A., & Emerson, C. P. (2007). SULF1 and SULF2 regulate heparan sulfate-mediated GDNF signaling for esophageal innervation. *Development*, 134(18), 3327–3338. doi:134/18/3327 [pii]. <https://doi.org/10.1242/dev.007674>
- Al Oustah, A., Danesin, C., Khouri-Farah, N., Farreny, M. A., Escalas, N., Cochard, P., ... Soula, C. (2014). Dynamics of sonic hedgehog signaling in the ventral spinal cord are controlled by intrinsic changes in source cells requiring sulfatase 1. *Development*, 141(6), 1392–1403. <https://doi.org/10.1242/dev.101717>
- Barnabé-Heider, F., Göritz, C., Sabelström, H., Takebayashi, H., Pfrieger, F. W., Meletis, K., & Frisén, J. (2010). Origin of new glial cells in intact and injured adult spinal cord. *Cell Stem Cell*, 7(4), 470–482. <https://doi.org/10.1016/j.stem.2010.07.014>
- Ben Haim, L., & Rowitch, D. H. (2017). Functional diversity of astrocytes in neural circuit regulation. *Nature Reviews. Neuroscience*, 18(1), 31–41. <https://doi.org/10.1038/nrn.2016.159>
- Bergles, D. E., & Richardson, W. D. (2015). Oligodendrocyte development and plasticity. *Cold Spring Harbor Perspectives in Biology*, 8(2), a020453. <https://doi.org/10.1101/cshperspect.a020453>
- Cahoy, J. D., Emery, B., Kaushal, A., Foo, L. C., Zamanian, J. L., Christopherson, K. S., ... Barres, B. A. (2008). A transcriptome database for astrocytes, neurons, and oligodendrocytes: A new resource for understanding brain development and function. *The Journal of Neuroscience*, 28(1), 264–278. <https://doi.org/10.1523/JNEUROSCI.4178-07.2008>
- Cai, J., Chen, Y., Cai, W. H., Hurlock, E. C., Wu, H., Kermie, S. G., ... Lu, Q. R. (2007). A crucial role for Olig2 in white matter astrocyte development. *Development*, 134(10), 1887–1899. <https://doi.org/10.1242/dev.02847>
- Danesin, C., & Soula, C. (2017). Moving the Shh source over time: What impact on neural cell diversification in the developing spinal cord? *Journal of Developmental Biology*, 5(2), 4. <https://doi.org/10.3390/jdb5020004>
- Deneen, B., Ho, R., Lukaszewicz, A., Hochstim, C. J., Gronostajski, R. M., & Anderson, D. J. (2006). The transcription factor NFIA controls the onset of gliogenesis in the developing spinal cord. *Neuron*, 52(6), 953–968. <https://doi.org/10.1016/j.neuron.2006.11.019>
- Dessaud, E., McMahon, A. P., & Briscoe, J. (2008). Pattern formation in the vertebrate neural tube: A sonic hedgehog morphogen-regulated transcriptional network. *Development*, 135(15), 2489–2503. <https://doi.org/10.1242/dev.009324>



- Dessaud, E., Yang, L. L., Hill, K., Cox, B., Ulloa, F., Ribeiro, A., ... Briscoe, J. (2007). Interpretation of the sonic hedgehog morphogen gradient by a temporal adaptation mechanism. *Nature*, 450(7170), 717–720. doi: nature06347 [pii]. <https://doi.org/10.1038/nature06347>
- Dhoot, G. K., Gustafsson, M. K., Ai, X., Sun, W., Standiford, D. M., & Emerson, C. P. (2001). Regulation of Wnt signaling and embryo patterning by an extracellular sulfatase. *Science*, 293(5535), 1663–1666. <https://doi.org/10.1126/science.293.5535.1663>
- El Masri, R., Seffouh, A., Lortat-Jacob, H., & Vivès, R. R. (2017). The "in and out" of glucosamine 6-O-sulfation: The 6th sense of heparan sulfate. *Glycoconjugate Journal*, 34(3), 285–298. <https://doi.org/10.1007/s10719-016-9736-5>
- Finzsch, M., Stolt, C. C., Lommes, P., & Wegner, M. (2008). Sox9 and Sox10 influence survival and migration of oligodendrocyte precursors in the spinal cord by regulating PDGF receptor alpha expression. *Development*, 135(4), 637–646. <https://doi.org/10.1242/dev.010454>
- Gallo, V., & Deneen, B. (2014). Glial development: The crossroads of regeneration and repair in the CNS. *Neuron*, 83(2), 283–308. <https://doi.org/10.1016/j.neuron.2014.06.010>
- Gong, S., Zheng, C., Doughty, M. L., Losos, K., Didkovsky, N., Schambra, U. B., ... Heintz, N. (2003). A gene expression atlas of the central nervous system based on bacterial artificial chromosomes. *Nature*, 425(6961), 917–925. <https://doi.org/10.1038/nature02033>
- Griemsmann, S., Höft, S. P., Bedner, P., Zhang, J., von Staden, E., Beinhauer, A., ... Steinhäuser, C. (2015). Characterization of Panglial gap junction networks in the thalamus, neocortex, and hippocampus reveals a unique population of glial cells. *Cerebral Cortex*, 25(10), 3420–3433. <https://doi.org/10.1093/cercor/bhu157>
- Guo, F., Maeda, Y., Ma, J., Delgado, M., Sohn, J., Miers, L., ... Pleasure, D. (2011). Macrogial plasticity and the origins of reactive astroglia in experimental autoimmune encephalomyelitis. *The Journal of Neuroscience*, 31(33), 11914–11928. <https://doi.org/10.1523/JNEUROSCI.1759-11.2011>
- Heintz, N. (2004). Gene expression nervous system atlas (GENSAT). *Nature Neuroscience*, 7(5), 483. <https://doi.org/10.1038/nn0504-483>
- Jiang, W., Ishino, Y., Hashimoto, H., Keino-Masu, K., Masu, M., Uchimura, K., ... Ikenaka, K. (2017). Sulfatase 2 modulates fate change from motor neurons to Oligodendrocyte precursor cells through coordinated regulation of Shh signaling with Sulfatase 1. *Developmental Neuroscience*, 39, 361–374. <https://doi.org/10.1159/000464284>
- Kanski, R., van Strien, M. E., van Tijn, P., & Hol, E. M. (2014). A star is born: New insights into the mechanism of astrogenesis. *Cellular and Molecular Life Sciences*, 71(3), 433–447. <https://doi.org/10.1007/s00018-013-1435-9>
- Karus, M., Denecke, B., French-Constant, C., Wiese, S., & Faissner, A. (2011). The extracellular matrix molecule tenascin C modulates expression levels and territories of key patterning genes during spinal cord astrocyte specification. *Development*, 138(24), 5321–5331. <https://doi.org/10.1242/dev.067413>
- Kuhlbrodt, K., Herbarth, B., Sock, E., Hermans-Borgmeyer, I., & Wegner, M. (1998). Sox10, a novel transcriptional modulator in glial cells. *The Journal of Neuroscience*, 18(1), 237–250.
- Lamanna, W. C., Kalus, I., Padva, M., Baldwin, R. J., Merry, C. L., & Dierks, T. (2007). The heparanome--The enigma of encoding and decoding heparan sulfate sulfation. *Journal of Biotechnology*, 129(2), 290–307. <https://doi.org/10.1016/j.jbiotec.2007.01.022>
- Liu, Y., & Rao, M. S. (2004). Glial progenitors in the CNS and possible lineage relationships among them. *Biology of the Cell*, 96(4), 279–290. <https://doi.org/10.1016/j.biolcel.2004.02.001>
- Lu, Q. R., Sun, T., Zhu, Z., Ma, N., Garcia, M., Stiles, C. D., & Rowitch, D. H. (2002). Common developmental requirement for olig function indicates a motor neuron/oligodendrocyte connection. *Cell*, 109(1), 75–86.
- Marshall, C. A., Novitsch, B. G., & Goldman, J. E. (2005). Olig2 directs astrocyte and oligodendrocyte formation in postnatal subventricular zone cells. *The Journal of Neuroscience*, 25(32), 7289–7298. <https://doi.org/10.1523/JNEUROSCI.1924-05.2005>
- Masahira, N., Takebayashi, H., Ono, K., Watanabe, K., Ding, L., Furusho, M., ... Ikenaka, K. (2006). Olig2-positive progenitors in the embryonic spinal cord give rise not only to motoneurons and oligodendrocytes, but also to a subset of astrocytes and ependymal cells. *Developmental Biology*, 293(2), 358–369. <https://doi.org/10.1016/j.ydbio.2006.02.029>
- Meijer, D. H., Kane, M. F., Mehta, S., Liu, H., Harrington, E., Taylor, C. M., ... Rowitch, D. H. (2012). Separated at birth? The functional and molecular divergence of OLIG1 and OLIG2. *Nature Reviews. Neuroscience*, 13(12), 819–831. <https://doi.org/10.1038/nrn3386>
- Nagamine, S., Tamba, M., Ishimine, H., Araki, K., Shiomi, K., Okada, T., ... Keino-Masu, K. (2012). Organ-specific sulfation patterns of heparan sulfate generated by extracellular sulfatases Sulf1 and Sulf2 in mice. *The Journal of Biological Chemistry*, 287(12), 9579–9590. <https://doi.org/10.1074/jbc.M111.290262>
- Nolte, C., Matyash, M., Pivneva, T., Schipke, C. G., Ohlemeyer, C., Hanisch, U. K., ... Kettenmann, H. (2001). GFAP promoter-controlled EGFP-expressing transgenic mice: A tool to visualize astrocytes and astrogliosis in living brain tissue. *Glia*, 33(1), 72–86.
- Ohayon, D., Garcès, A., Joly, W., Soukkaieh, C., Takagi, T., Sabourin, J. C., ... Pattyn, A. (2016). Onset of spinal cord astrocyte precursor emigration from the ventricular zone involves the Zeb1 transcription factor. *Cell Reports*, 17(6), 1473–1481. <https://doi.org/10.1016/j.celrep.2016.10.016>
- Orthmann-Murphy, J. L., Abrams, C. K., & Scherer, S. S. (2008). Gap junctions couple astrocytes and oligodendrocytes. *Journal of Molecular Neuroscience*, 35(1), 101–116. <https://doi.org/10.1007/s12031-007-9027-5>
- Pringle, N. P., & Richardson, W. D. (1993). A singularity of PDGF alpha-receptor expression in the dorsoventral axis of the neural tube may define the origin of the oligodendrocyte lineage. *Development*, 117(2), 525–533.
- Pringle, N. P., Yu, W. P., Howell, M., Colvin, J. S., Ornitz, D. M., & Richardson, W. D. (2003). Fgfr3 expression by astrocytes and their precursors: Evidence that astrocytes and oligodendrocytes originate in distinct neuroepithelial domains. *Development*, 130(1), 93–102.
- Rosen, S. D., & Lemjabbar-Alaoui, H. (2010). Sulf-2: An extracellular modulator of cell signaling and a cancer target candidate. *Expert Opinion on Therapeutic Targets*, 14, 935–949. <https://doi.org/10.1517/14728222.2010.504718>
- Rowitch, D. H., & Kriegstein, A. R. (2010). Developmental genetics of vertebrate glial-cell specification. *Nature*, 468(7321), 214–222. <https://doi.org/10.1038/nature09611>
- Takebayashi, H., Nabeshima, Y., Yoshida, S., Chisaka, O., & Ikenaka, K. (2002). The basic helix-loop-helix factor olig2 is essential for the development of motoneuron and oligodendrocyte lineages. *Current Biology*, 12(13), 1157–1163.
- Tien, A. C., Tsai, H. H., Molofsky, A. V., McMahon, M., Foo, L. C., Kaul, A., ... Rowitch, D. H. (2012). Regulated temporal-spatial astrocyte precursor cell proliferation involves BRAF signalling in mammalian spinal cord. *Development*, 139(14), 2477–2487. <https://doi.org/10.1242/dev.077214>
- Touhri, Y., Escalas, N., Benazerf, B., Cochard, P., Danesin, C., & Soula, C. (2012). Sulfatase 1 promotes the motor neuron-to-oligodendrocyte fate switch by activating Shh signaling in Olig2 progenitors of the embryonic ventral spinal cord. *The Journal of Neuroscience*, 32(50), 18018–18034. <https://doi.org/10.1523/JNEUROSCI.3553-12.2012>
- Tran, T. H., Shi, X., Zaia, J., & Ai, X. (2012). Heparan sulfate 6-O-endosulfatases (Sulfs) coordinate the Wnt signaling pathways to regulate myoblast fusion during skeletal muscle regeneration. *The Journal of Biological Chemistry*, 287(39), 32651–32664. <https://doi.org/10.1074/jbc.M112.353243>

- Trinh, I. A., McCutchen, M. D., Bonner-Fraser, M., Fraser, S. E., Bumm, L. A., & McCauley, D. W. (2007). Fluorescent in situ hybridization employing the conventional NBT/BCIP chromogenic stain. *Bio-Techniques*, 42(6), 756–759. <https://doi.org/10.2144/000112476>
- Tsai, H. H., Li, H., Fuentealba, L. C., Molofsky, A. V., Taveira-Marques, R., Zhuang, H., ... Rowitch, D. H. (2012). Regional astrocyte allocation regulates CNS synaptogenesis and repair. *Science*, 337(6092), 358–362. <https://doi.org/10.1126/science.1222381>
- Ventéo, S., Bourane, S., Méchaly, I., Sar, C., Abdel Samad, O., Puech, S., ... Carroll, P. (2012). Regulation of the Na,K-ATPase gamma-subunit FXD2 by Runx1 and ret signaling in normal and injured non-peptidergic nociceptive sensory neurons. *PLoS ONE*, 7(1), e29852. <https://doi.org/10.1371/journal.pone.0029852>
- Zhao, X., Chen, Y., Zhu, Q., Huang, H., Teng, P., Zheng, K., ... Qiu, M. (2014). Control of astrocyte progenitor specification, migration and maturation by Nkx6.1 homeodomain transcription factor. *PLoS ONE*, 9(10), e109171. <https://doi.org/10.1371/journal.pone.0109171>
- Zhou, Q., & Anderson, D. J. (2002). The bHLH transcription factors OLIG2 and OLIG1 couple neuronal and glial subtype specification. *Cell*, 109(1), 61–73.
- Zhou, Q., Wang, S., & Anderson, D. J. (2000). Identification of a novel family of oligodendrocyte lineage-specific basic helix-loop-helix transcription factors. *Neuron*, 25(2), 331–343.

How to cite this article: Ohayon D, Escalas N, Cochard P, Glise B, Danesin C, Soula C. Sulfatase 2 promotes generation of a spinal cord astrocyte subtype that stands out through the expression of Olig2. *Glia*. 2019;67:1478–1495. <https://doi.org/10.1002/glia.23621>